Spatial processing for coherent noise reduction in ultrasonic imaging

Nihat M. Bilgutay, Rashmi Murthy, and Uthai Bencharit
ECE Department, Drexel University, Philadelphia, Pennsylvania 19104

Jafar Saniie
ECE Department, Illinois Institute of Technology, Chicago, Illinois 60616

(Received 4 April 1988; accepted for publication 15 September 1989)

When the target is received in the presence of coherent noise resulting from a large number of complex and randomly distributed scatterers inherent to the medium, the ability of the system to distinguish between the two types of signals often becomes the most crucial performance consideration. Conventional techniques that are capable of suppressing time-varying (incoherent) noise are generally not effective when the noise is time invariant (coherent). In recent years, diversity techniques have been developed that allow the decorrelation of the coherent noise term by altering either the transmitted frequency or the position of the transducer. Although the diversity techniques provide some noise suppression when used in conjunction with the conventional averaging algorithms, their potential benefits cannot be fully exploited by such linear techniques alone. In the work presented here, a nonlinear detection scheme based on the polarity of the spatially decorrelated signals is examined. The theoretical and experimental results indicate that the polarity-thresholding algorithm provides target enhancement that is far superior to the linear techniques previously used in spatial processing. Furthermore, the paper examines the spatial decorrelation properties of the experimental data to determine the desirable parameters for data acquisition and signal processing.

PACS numbers: 43.60.Gk, 43.35.Zc

INTRODUCTION

In recent years, ultrasonic nondestructive testing (NDT) has become one of the most predominant and popular methods of quality assurance for a wide range of applications because of its feasibility, versatility, and effectiveness. However, the quality of ultrasonic images is often severely limited when the level of echoes from the surrounding unwanted reflectors is comparable to or larger than that of the target signal. Such background noise is not unique to any specific system but plagues a diverse range of imaging and detection applications involving radar, optics, sonar, and ultrasound. The backscattered signal from reflectors in the vicinity of the desired target is known as clutter in radar, grain noise in material evaluation, and speckle in tissue characterization and optics. This type of noise generally results from randomly distributed scatterers that are small compared to the transmitted wavelength and hence cannot be resolved. However, the resulting interference pattern is often difficult to distinguish from the desired target signal. Furthermore, since the echoes from stationary scatterers exhibit no phase or amplitude variation with time (i.e., coherent), they cannot be suppressed by time averaging. However, it is possible to decorrelate the clutter echoes by shifting either the transmitted frequency (i.e., frequency diversity) or the position of the transmitter/receiver (i.e., spatial diversity). The diversity techniques affect the target echoes to a much lesser extent when the target size is significantly larger than clutter causing scatterers, which generally is the case in practice. Therefore, by varying the position or the frequency of the transmitter, the clutter can be made to behave like time-varying noise (uncorrelated) while the target echoes remain virtually unchanged (correlated). Consequently, processing the resulting signal ensemble can improve the signal-to-noise ratio. This fundamental principle was applied using conventional averaging techniques both in radar[1–3] and ultrasonic[4,5] applications. In later work, two novel nonlinear algorithms were developed (i.e., minimization and polarity-thresholding algorithms) and used in conjunction with a spectral diversity technique known as split-spectrum processing.[6–12]

The work presented here focuses on the application of the polarity-thresholding algorithm to spatially decorrelated data.[13–14] The performance of the polarity-thresholding algorithm is examined both theoretically and experimentally relative to the linear averaging technique, which is widely used in conventional spatial processing. The spatial data acquisition and signal-processing parameters are also analyzed to optimize the performance of the algorithms for ultrasonic nondestructive testing and imaging of materials.

I. SIGNAL-PROCESSING ALGORITHMS

Grain echo decorrelation can be achieved by viewing the target from different locations, which can be accomplished by either physically shifting the transducer or employing an array of equally spaced transducers. The objective is to obtain a set of decorrelated A scans with a minimal loss of lateral resolution. The spatial processing algorithms can achieve flaw enhancement by distinguishing and emphasizing the differences in the behavior of the grain and flaw echoes to shifts in the transducer location. When the defect of

 0001-4966/90/020728-09$00.80

interest is much larger than the average grain size, a shift in the transducer location by a fraction of the element diameter will have a relatively minor affect on the flaw signal, but in a resolution cell containing a large number of grains, the resultant grain interference pattern can vary significantly. The sensitivity of grain echoes to spatial shifts in the transducer location will be determined by many complex factors such as transducer frequency, beam pattern, scattering and material properties, attenuation, etc. Since the correlation between A scans is proportional to the amount of ultrasonic beam overlap, the optimal spatial processing parameters will be governed by the frequency and geometrical properties of the transducer (i.e., spacing, diameter, focal length, etc.).

If the spatial data consist of N individual A scans corresponding to different but equally spaced locations on the sample, each with M data points, the corresponding data can be represented by an $N \times M$ matrix whose columns consist of spatially decorrelated data corresponding to fixed time instants (or sample depth). The noise suppression algorithms recombine or process the data in each column to obtain an enhanced flaw signal.[13,14] The conventional technique that has been used in processing spatial data is known as linear averaging (LA) where the output is obtained by determining the average value of the spatial data in each column. Therefore, the output of LA can be defined as

$$y_{\mathrm{LA}}(t_k) = \frac{1}{N}\sum_{i=1}^{N} r_i(t_k), \tag{1}$$

where $r_i(t)$ is the received signal from the ith transducer position and t_k; $k = 1,2,...,M$ are the discrete time instants. In this paper, LA will primarily be used as a reference for evaluating the performance of the nonlinear polarity-thresholding (PT) algorithm.

The PT algorithm was originally proposed for spectral processing of ultrasonic signals[12] and subsequently used in conjunction with the split-spectrum technique for both flaw detection and imaging.[13–16] The PT algorithm is based on the principle that, at time instants where the flaw signal is present, the corresponding spatial data will not exhibit any polarity reversal since the flaw will dominate the grain noise (i.e., all the elements of the corresponding column will have the same polarity). However, if the spatial data at time t_k contains only grain noise, which is zero mean, then it is likely that the data will exhibit polarity reversal. Therefore, the grain noise level can be reduced significantly by setting the amplitude of the processed signal to zero at time instants where polarity reversal occurs while assigning the value of the reference signal [or some processed value for the data $r_i(t)$; $i = 1,2,...,N$] when the data has identical polarity. Hence, the PT output can be expressed as

$$y_{\mathrm{PT}}(t_k) = \begin{cases} y(t_k) \text{ if } r_i(t_k) > 0 \text{ or } r_i(t_k) < 0, \\ \text{for all } i = 1,2,...,N, \\ 0, \quad \text{otherwise}, \end{cases} \tag{2}$$

where t_k are discrete time instants with $k = 1, 2,...,M$ and $y(t_k)$ is the value of the reference signal corresponding to one of the spatial data $r_i(t)$; $i = 1,2,...,N$ or to their processed value obtained by an appropriate algorithm. For example, if the nonzero portion of the PT output is obtained by averaging the spatial data, then $y(t_k) = y_{\mathrm{PT}}(t_k)$ as defined by Eq. (1).

The theoretical performance of these algorithms was previously examined for spectral processing.[13–16] In the spectral case, the derivation is based on the assumption that the decorrelated signals are obtained by dividing the available spectrum of B Hz into N-nonoverlapped bands with equal widths (i.e., B/N). Therefore, in split-spectrum processing, the number of decorrelated signals can be increased only at the expense of reducing their bandwidths. By contrast, in spatial processing, decorrelation is achieved by merely shifting the position of the transducer while maintaining the original bandwidth. Therefore, although the two techniques are similar in principle, the behavior of their performance curves as a function of the number of windows N is markedly different. Furthermore, since the spatially decorrelated signals maintain the original bandwidth, spatial processing is less likely to result in any loss of resolution, provided that the data are acquired within a relatively small spatial region. However, it should be noted, that in spatial processing, the data corresponding to each spatial location must be acquired and stored individually, which is more time consuming and requires larger computer memory than spectral processing.

II. THEORETICAL PERFORMANCE OF ALGORITHMS

The performance of the PT and LA algorithms will be based on the classical signal-to-noise ratio (SNR) definitions, with the assumption that the separation between the spatial locations is sufficiently large to yield independent grain echoes. This approach affords mathematical simplicity without loss of generality. However, it should be noted that in practice this condition may be relaxed to achieve larger number of spatial data. Although the theoretical derivations presented here are based on one-dimensional data for simplicity, the results are also directly applicable to imaging.

Since the received signal $r_i(t)$ is assumed to be a random process, its value at a particular time instant $t = t_0$ will be a random variable $r_i = r_i(t_0)$. The SNR derivations are based on the following hypothesis testing model, where the observation time $t = t_0$ is assumed to coincide with the peak value of the defect echo (when defect is present) so that the observed signal may be represented as

$$\begin{aligned} &H_1\colon\ r_i = m + n_i, \text{ defect present}, \\ &H_0\colon\ r_i = n_i, \text{ no defect}, \end{aligned} \tag{3}$$

where m is the peak value of the flaw echo, and n_i; $i = 1,2,...,N$ are the independent and identically distributed (iid) zero-mean Gaussian random variables representing the grain noise component of the received signal from the ith transducer position. Since the noise terms n_i are zero mean, their standard deviation and rms values are identical.

The SNR for the received signals $r_i(t)$; $i = 1,2,...,N$ is defined as[13]

$$(\mathrm{SNR})|_r = E[r_i|H_1]/\mathrm{rms}[r_i|H_0] \tag{4}$$

where $E[\ ]$ and rms denote the expected and the root-mean-square values, respectively. The above SNR definition is

based on the magnitude ratio rather than the more conventional power ratio since, in ultrasonic applications, the magnitude terms are generally displayed. However, if the SNR value in terms of power is desired, this can also be derived similarly.[10] From Eqs. (3) and (4), the SNR for the received signal can be determined as

$$(\mathrm{SNR})|_r = \frac{E[m+n_i]}{\mathrm{rms}[n_i]} = \frac{m}{\sqrt{E[n_i^2]}} = \frac{m}{\sigma}, \tag{5}$$

where m is the peak signal amplitude and σ is the standard deviation of the noise terms.

The signal-to-noise ratio enhancement (SNRE) provides a measure of the improvement at the output of the process with respect to the input:

$$\mathrm{SNRE} = (\mathrm{SNR})|_{\mathrm{out}}/(\mathrm{SNR})|_{\mathrm{in}}, \tag{6}$$

where $(\mathrm{SNR})|_{\mathrm{in}}$ is defined by Eq. (5) if the input to the process is $r_i(t)$; $i = 1,2,\ldots, N$. The SNRE for the PT and LA algorithms are calculated below based on Eqs. (3)–(6).

A. SNRE for the polarity-thresholding algorithm

The SNR at the output of the PT algorithm can be determined using Eq. (4) as

$$\mathrm{SNR}|_{\mathrm{PT}} = E[y_{\mathrm{PT}}|H_1]/\mathrm{rms}[y_{\mathrm{PT}}|H_0], \tag{7}$$

where y is the output of the PT algorithm. The $(\mathrm{SNR})|_{\mathrm{PT}}$ can be calculated using basic probability concepts. The positive and negative polarity probabilities for the received signal for hypothesis H_1 are, respectively,

$$p_{H_1} = P(r_i \geqslant 0|H_1) = P(n_i \geqslant -m)$$

$$= \frac{1}{\sqrt{2\pi}\sigma}\int_{-m}^{\infty} e^{-n^2/2\sigma^2}dn$$

$$= \frac{1}{2} + \frac{1}{\sqrt{2\pi}\sigma}\int_0^m e^{-n^2/2\sigma^2}dn = \frac{1}{2} + \frac{1}{2}\,\mathrm{erf}\left(\frac{m}{\sqrt{2}\sigma}\right) \tag{8}$$

and

$$q_{H_1} = P(r_i < 0|H_1) = 1 - p_{H_1} = \frac{1}{2} - \frac{1}{2}\,\mathrm{erf}\left(\frac{m}{\sqrt{2}\sigma}\right), \tag{9}$$

where the error function is defined as

$$\mathrm{erf}(x) = \frac{2}{\sqrt{\pi}}\int_0^x e^{-u^2}du. \tag{10}$$

Similarly, for hypothesis H_0, the positive and negative polarity probabilities are, respectively,

$$p_{H_0} = P(r_i \geqslant 0|H_0) = P(n_i \geqslant 0)$$

$$= \frac{1}{\sqrt{2\pi}\sigma}\int_0^{\infty} e^{-n^2/2\sigma^2}dn = \frac{1}{2} \tag{11}$$

and

$$q_{H_0} = 1 - p_{H_0} = \tfrac{1}{2}. \tag{12}$$

Since the data obtained from the N spatial locations at fixed time instants are assumed to be independent (i.e., independent trials) with fixed probabilities (between trials), the probabilities governing the combinatorial outcomes for signal polarity, which is binary, can be determined based on Bernoulli trials.[17] Hence, the probability that, at any instant of time $t = t_0$, k out of N-independent spatial data will exhibit positive polarity can be defined as

$$P_N(k) = \binom{N}{k}p^k q^{N-k}, \tag{13}$$

with binomial coefficient

$$\binom{N}{k} = \frac{N!}{k!(N-k)!},$$

where p and $q = 1 - p$ are the probabilities of positive and negative polarities, respectively, as defined above for hypotheses H_1 and H_0. Therefore, from Bernoulli trials, it is clear that there are only two possible ways polarity reversal will not occur for the spatial data: when the N signals are either all positive [i.e., $P_N(k = N)$] or all negative [i.e., $P_N(k = 0)$]. Therefore, from Eqs. (8), (9), and (13), the probability of *no polarity reversal* for hypothesis H_1 can be calculated as

$$P(\mathrm{NPR}|H_1) = P_N(k = N|H_1) + P_N(k = 0|H_1)$$

$$= p_{H_1}^N + q_{H_1}^N \tag{14}$$

$$= \left[\frac{1}{2} + \frac{1}{2}\,\mathrm{erf}\left(\frac{m}{\sqrt{2}\sigma}\right)\right]^N + \left[\frac{1}{2} - \frac{1}{2}\,\mathrm{erf}\left(\frac{m}{\sqrt{2}\sigma}\right)\right]^N.$$

Similarly, the probability of no polarity reversal for hypothesis H_0 can be calculated from Eqs. (11)–(13):

$$P(\mathrm{NPR}|H_0) = P_N(k = N|H_0) + P_N(k = 0|H_0)$$

$$= (1/2)^N + (1/2)^N = 2^{(1-N)}. \tag{15}$$

Since the PT output is set to zero at time instants where the spatial data exhibit polarity reversal, the mean value of the PT output will be equal to the mean value of the processes data times the probability of no polarity reversal. Recall that, when there is no polarity reversal, the PT output is determined by processing the spatial data or by simply setting it equal to the reference signal value. Therefore, for hypothesis H_1, the mean value of PT output becomes

$$E[y_{\mathrm{PT}}|H_1] = P(\mathrm{NPR}|H_1)E[y_{\mathrm{NPR}}|H_1], \tag{16}$$

where $E[y_{\mathrm{NPR}}|H_1]$ is the mean value of the processed spatial data when no polarity reversal occurs. Similarly, for hypothesis H_0, the noise power at the PT output will be equal to the power (rms) of the processed data times the polarity of no polarity reversal. Therefore, for hypothesis H_0, the rms value of PT output becomes

$$\mathrm{rms}[y_{\mathrm{PT}}|H_0] = [P(\mathrm{NPR}|H_0)]^{1/2}\mathrm{rms}[y_{\mathrm{NPR}}|H_0], \tag{17}$$

where rms $[y_{\mathrm{NPR}}|H_0]$ is the rms value of the processed spatial data when no polarity reversal occurs. Therefore, from Eqs. (7), (16), and (17), the SNR for PT becomes

$$(\mathrm{SNR})|_{\mathrm{PT}} = \{P(\mathrm{NPR}|H_1)/[P(\mathrm{NPR}|H_0)]^{1/2}\}(\mathrm{SNR})|_{\mathrm{NPR}}, \tag{18}$$

where $P(\mathrm{NPR}|H_1)$ and $P(\mathrm{NPR}|H_0)$ are defined by Eqs. (14) and (15), respectively. Note that $(\mathrm{SNR})|_{\mathrm{NPR}}$ will be determined by the choice of processing performed on the spatial data $r_i(t)$ when they exhibit no polarity reversal (i.e.,

the SNR of the process, such as LA). Therefore, the SNRE for PT with respect to $(\mathrm{SNR})|_{\mathrm{NPR}}$ becomes

$$(\mathrm{SNRE})|_{\mathrm{PT}} = \frac{(\mathrm{SNR})|_{\mathrm{PT}}}{(\mathrm{SNR})|_{\mathrm{NPR}}} = \frac{P(\mathrm{NPR}|H_1)}{[P(\mathrm{NPR}|H_0)]^{1/2}}. \quad (19)$$

Finally, from Eqs. (14), (15), and (19), the SNRE for PT can be expressed as

$$(\mathrm{SNRE})|_{\mathrm{PT}} = \frac{[1+\mathrm{erf}(m/\sqrt{2}\sigma)]^N + [1-\mathrm{erf}(m/\sqrt{2}\sigma)]^N}{2^{(N+1)/2}}. \quad (20)$$

The $(\mathrm{SNRE})|_{\mathrm{PT}}$ with respect to the reference signal $r_i(t)$ can be found by multiplying Eq. (20) by the ratio $(\mathrm{SNR})|_{\mathrm{NPR}}/(\mathrm{SNR})|_r$, where the denominator is given by Eq. (5).

B. SNRE for the linear averaging algorithm

The SNRE for LA can be derived similarly using Eqs. (1), (5), and (6). The SNR for LA is defined as

$$(\mathrm{SNR})|_{\mathrm{LA}} = E[y_{\mathrm{LA}}|H_1]/\mathrm{rms}[y_{\mathrm{LA}}|H_0]. \quad (21)$$

Since LA is obtained by averaging the independent data from N spatial locations as defined by Eq. (1), the SNR at the output of LA becomes

$$(\mathrm{SNR})|_{\mathrm{LA}} = E\left(\frac{1}{N}\sum_{i=1}^{N}(m+\tilde{n}_i)\right)\Big/\sqrt{E\left(\frac{1}{N}\sum_{i=1}^{N}n_i\right)^2}$$

$$= \frac{m}{\sigma/\sqrt{N}} = \frac{\sqrt{N}\,m}{\sigma}. \quad (22)$$

The SNRE for LA can be obtained from Eqs. (5) and (22) as

$$(\mathrm{SNRE})|_{\mathrm{LA}} = (\mathrm{SNR})|_{\mathrm{LA}}/(\mathrm{SNR})|_r = \sqrt{N}, \quad (23)$$

where the SNR for the received signals $(\mathrm{SNR})|_r = m/\sigma$ as defined in Eq. (5). Thus the SNRE achieved by linearly averaging N-independent spatial data will be $N^{1/2}$, which is a well-known result (i.e., the noise rms value reduces by $N^{1/2}$ when N-independent terms are averaged). Note that, unlike PT, the SNRE for LA does not depend on the value of the input SNR.

C. Interpretation of the theoretical curves

It can be seen from Eq. (20) and Fig. 1 that the signal-to-noise ratio enhancement for PT is a function of both the number of independent signals N and the input SNR m/σ. For $m/\sigma > 0.9$, the algorithm provides improvement in the output SNR for any N. For $m/\sigma \leqslant 0.5$, the output SNR decreases even for large N. For input SNR between these values (i.e., $0.5 < m/\sigma < 0.9$), there is no improvement for small N values, but the SNRE improves dramatically as N increases. Although, for fixed N, the performance of the PT algorithm saturates as the input SNR approaches 3, significant improvement can be obtained at these input SNR values, provided a sufficient number of independent samples are available as shown in Fig. 1. However, in practice, the number of independent samples N will be limited by the geometry and physical parameters governing the system and defect.

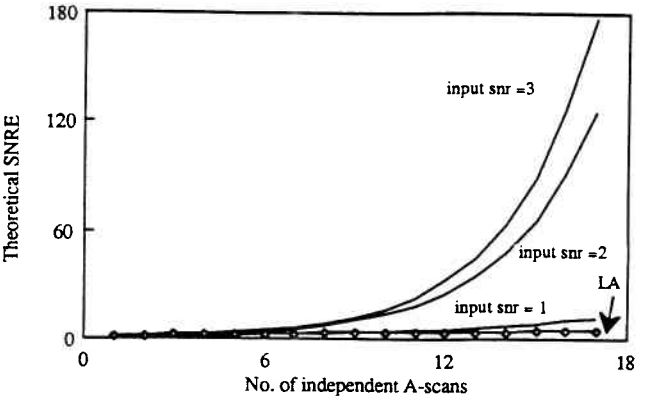

FIG. 1. Plot of theoretical SNRE versus number of independent A scans.

In contrast to the above observations, SNRE for LA is independent of the input SNR and provides a steady, but relatively minor improvement with N, which can be seen from Eq. (23).

III. CORRELATION COEFFICIENT FOR SPATIAL DATA

A. Data acquisition procedure and test samples

The data acquisition system used a 125-MHz LeCroy 9400 digital oscilloscope. The data are collected by moving the transducer in a raster scan over a rectangular region of the sample. A MASSCOMP MC-5500 computer is used to control the data acquisition process and perform signal processing. The transducer moves in incremental steps of equal size and its motion is synchronized by the computer. A 1/2-in.-diam unfocused KB-Aerotech transducer of center frequency 5 MHz was used to collect the data. The sample was immersed in a water bath and the measurements were made in the farfield of the transducer. The data were time averaged 60 times at each transducer position in order to reduce incoherent system noise prior to processing, resulting in slightly higher input SNR. A sampling frequency of 50 MHz was used to collect the data. The samples used are cylindrical shaped, type 303 heat treated austenitic stainless steel with average grain sizes ranging between 75 and 106 μm, which were measured using the linear intercept method. The samples have been labeled SST25, SST50, and SST75, corresponding to their heat treatment temperatures of 1325, 1350, and 1375 °C, respectively. The target is a flat-bottomed hole drilled perpendicular to the top of the sample with diameter of 3.2 mm for the SST25 sample and a diameter of 4.2 mm for the SST50 and SST75 samples. Thus the hole has a diameter larger than the ultrasonic wavelength (i.e., $\lambda \cong 1$ mm), causing the flaw to behave as a geometric reflector. Since the wavelength of the incident pulse is much larger than the average grain size, the grains act as Rayleigh scatterers.

The spatial processing involves the combining of multiple neighboring A scans obtained from equidistant locations within a specified region called the spatial window. A typical spatial window consisting of nine A scans (i.e., 3×3) is shown in Fig. 2. The raw data used to obtain the processed images comprise equally spaced parallel B scans. Each B scan consists of 64 equally spaced A scans positioned along a

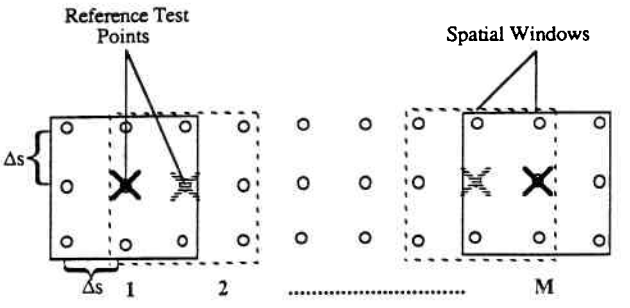

FIG. 2. Typical spatial window for B-scan processing.

straight line, each containing 512 points. Therefore, the unprocessed data consist of a matrix of equally spaced ($\Delta s = 0.305$ mm) A scans which are processed to yield a single B scan (64×512). The spatially decorrelated A scans within the spatial window are processed, and the resulting A scan is recorded at the center of the window (the reference point). Next, the spatial window is shifted by a single point as illustrated by a 3×3 spatial window in Fig. 2, and the algorithms are applied to the resulting data. The process is repeated until a single compounded B-scan image results.

B. Effect of spatial shift on data correlation

In previous work,[18,19] the correlation between neighboring A scans has been investigated both theoretically and experimentally. The results show that, in order to achieve total decorrelation, a translation distance of more than one transducer diameter is necessary between adjacent A scans. Since this separation produces a severe loss of lateral resolution, in practice A scans with correlation coefficients of $\rho \leqslant 0.2$ are generally considered to be sufficiently decorrelated for processing. Taking this into consideration, Burckhardt[19] and Gehlbach[20] have theoretically shown that translation distances of 1/2 and 1/3 of the transducer diameter, respectively, would provide sufficient decorrelation. Experimentally, Trahey *et al.*[21] predicted that a translation of approximately 40% of the transducer aperture length would be sufficient. Typical A scans of grain noise with and without the flaw signal are shown in Figs. 3 and 4, respectively. The correlation coefficient for two A scans was calculated using

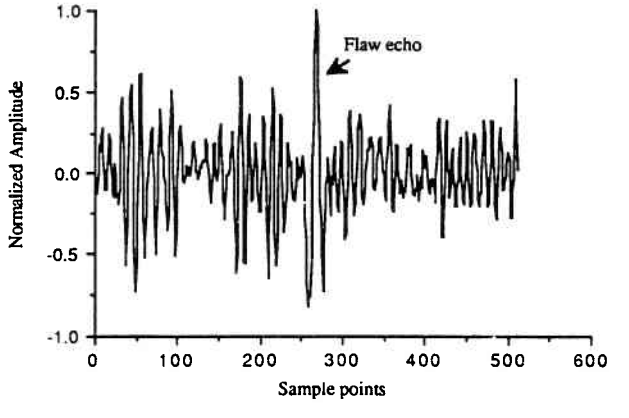

FIG. 3. A scan with flaw echo embedded in grain noise.

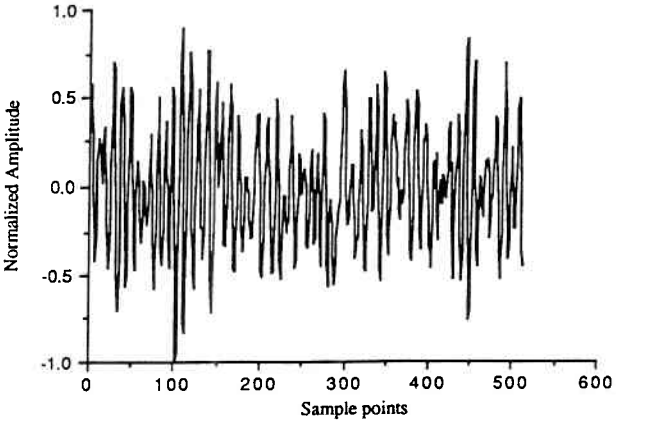

FIG. 4. A scan corresponding to grain noise only.

$$\rho = \frac{1/N \sum_{i=1}^{N} (x_i - \bar{x})(y_i - \bar{y})}{\sqrt{1/N \sum_{i=1}^{N} (x_i - \bar{x})^2 1/N \sum_{j=1}^{N} (y_j - \bar{y})^2}}, \quad (24)$$

where $\bar{x}$ and $\bar{y}$ are the mean amplitude values for the two A scans.

Figure 5 shows the decorrelation distances for stainless steel samples with different grain sizes, where each plot represents the average correlation coefficient values corresponding to *flaw signal + grain noise* (i.e., $S + N$) and the *grain noise only* cases. The plots correspond to data obtained in the farfield using a 1/2-in. (12.7-mm) diameter, unfocused KB-Aerotech Alpha transducer with center frequency 5 MHz. Although the target echo spans only a single range cell, it can be seen from Fig. 5 that the target + noise case shows a higher correlation than the noise only case. Therefore, linear or nonlinear processing of data obtained from sufficiently spaced transducer locations leads to reduction in clutter (i.e., grain noise), while the flaw signal remains relatively unaffected.

The decorrelation of grain noise with translation distance depends strongly on various transducer parameters such as center frequency, bandwidth, diameter, focal length (for focused transducers), distance to the sample, as well as material properties like average grain size. Therefore, the decorrelation distances reported in literature show wide variation ranging up to 1/2 the transducer diameter.[19–21] For the samples examined here, significant decorrelation was observed beyond 2-mm separation, with correlation coefficient ranging between 0% and 40%.

The derivations for SNRE given in the previous section assume that the A scans are totally uncorrelated, which is not the case in practice. The two critical parameters that govern the performance of spatial processing (and, hence, determine the effective number of independent A scans present in the raw data) are the spatial window dimensions and the transducer spacing. To maintain the resolution and prevent flaw echo suppression in the processed image, the two parameters must be selected carefully. In general, experimental measurements will be made with transducer spacing much less than the value required for complete grain echo decorrelation, and using a relatively small spatial window size. Consequently, the enhancement does not depend solely on the

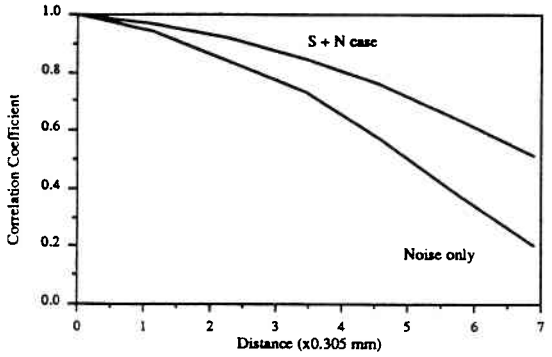

(a) SST25

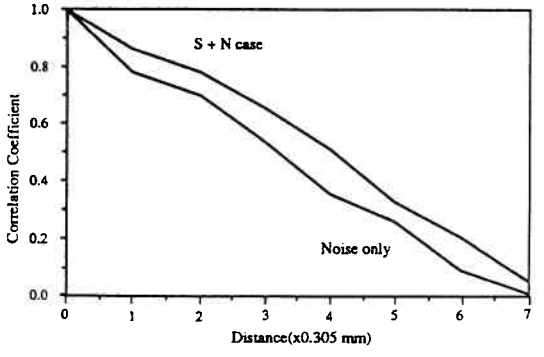

(b) SST50

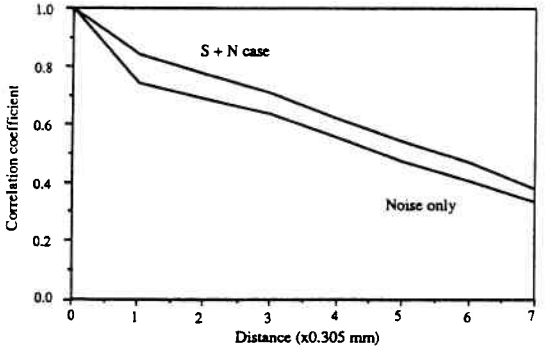

(c) SST75

FIG. 5. Decorrelation curves for different stainless steel samples.

total number of signals obtained within the spatial window, but on the number of effective (totally correlated) A scans within it.

It was observed experimentally that, for the stainless steel samples used here, the flaw echo amplitude falls to 75% of its peak value at a distance of approximately 3 mm. When the flaw echo is present, it is essential that the individual A scans used for processing have some minimum flaw amplitude for the output to maintain and enhance the flaw echo. If we consider 75% of the peak flaw amplitude as the minimum necessary level for each A scan, spatial window for data acquisition should be limited to an area of 6×6 mm around the flaw. Furthermore, the spacing between the adjacent reference points must be relatively small (i.e., as compared to the dimension of the spatial region). This will ensure that the flaw signal is not inadvertently lost or the resolution markedly reduced as a result of processing, especially when nonlinear techniques are used.

For the ideal case ($\rho = 0$), the theoretical improvement in SNR for LA technique was shown to be $N^{1/2}$, where N is the number of independent A scans used for processing. However, due to the practical limitations imposed on the spatial window size, N will be relatively small and generally much smaller than the number of total A scans within the spatial window. Consequently, the enhancement provided by LA will generally be insufficient. Thus the use of nonlinear algorithms such as PT becomes crucial when the acquired A scans are significantly correlated such that the number of independent A scans N is relatively small.

IV. EXPERIMENTAL RESULTS AND DISCUSSION

The algorithms were experimentally tested using the data required from the stainless steel samples described earlier, namely, SST25, SST50, and SST75, with average grain sizes of 75, 86, and 106 μm, respectively. The flat-bottom hole in the SST25 sample is located at a depth of 60.5 mm within the sample and has a diameter of 3.2 mm. The flat-bottom holes in the SST50 and SST75 samples are both 4.2 mm in diameter and are located at a depth of 67.1 mm.

Figures 6 and 7 show processed results corresponding to the SST50 sample (input SNR $\cong$ 5.2) and the SST75 sample (input SNR $\cong$ 2.8). The PT algorithm performs extremely well in improving the signal-to-noise ratio and is especially successful for the SST75 sample where the unprocessed image shows high-level grain echoes, which correspond to low-input SNR regions. The output SNR improves as the window size becomes larger (i.e., with increasing number of independent A scans within the spatial window) and a clutter-free image of the flaw results from the application of an 11×11 window for both the SST50 and SST75 samples. Assuming a decorrelation distance of 1.8 mm for the SST50 sample, where the individual A scans are evenly spaced at 0.305 mm, the estimated number of spatially independent A scans for a 11×11 spatial window is 8. Similarly, for the SST75 sample with a decorrelation distance of 2.4 mm, the number of A scans that can be assumed independent is 6.

It can be concluded from the experimental results that PT provides a significant improvement over LA as expected from the theoretical derivations. The LA output is shown here only for the 11×11 case, which yields the best results for linear averaging. However, it is clear that LA provides some improvement especially for the SST75 sample (see Fig. 7) where the high-level grain echoes are reduced. However, unlike PT, LA is unable to remove the remaining background grain noise. Similar results were also obtained for the SST25 data, which are not displayed here.

The size of the spatial window is an important parameter and was observed to become more critical as the sample grain size increases. The probability of phase reversals for the flaw echo increases as the spacing between A scans becomes larger (i.e., for larger spatial window size). This becomes more significant for larger grained samples, most likely due to increasing grain noise and multiple scattering

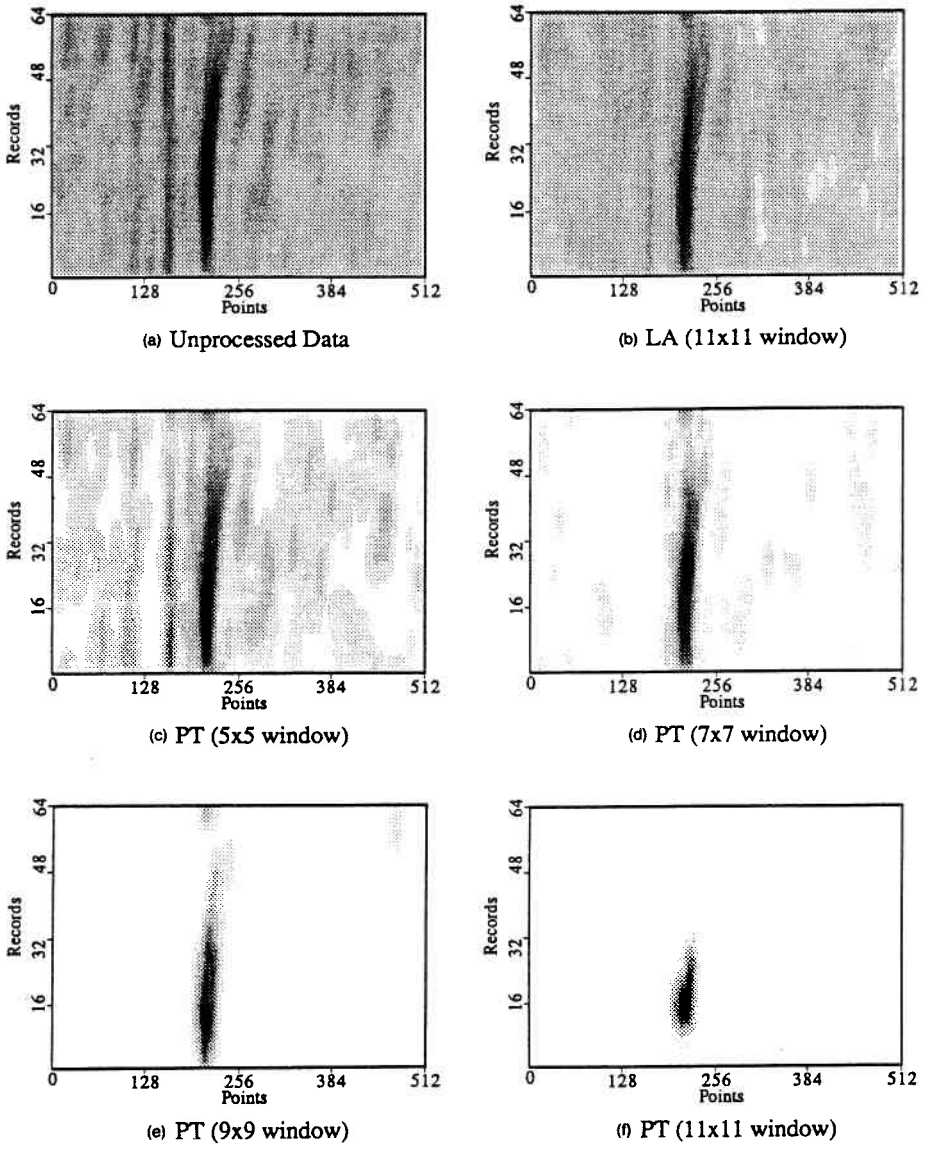

(a) Unprocessed Data (b) LA (11x11 window)

(c) PT (5x5 window) (d) PT (7x7 window)

(e) PT (9x9 window) (f) PT (11x11 window)

FIG. 6. Unprocessed and spatially processed SST50 stainless data for LA and PT.

effects, thus raising the possibility of "zeroing" the flaw at a particular reference pixel as the size of the spatial window is increased. Therefore, a trade-off must be made between SNR of the resulting image and the risk of losing the flaw when large spatial windows are used.

The spacing between adjacent A scans is also an important parameter of interest in data collection and was experimentally observed to affect the performance of the PT algorithm. Although the performance of the algorithm is ultimately limited by the effective number of independent A scans within a fixed spatial region, from statistical considerations, increasing the number of A scans within this region will improve the probability of detecting a phase reversal. This factor becomes more crucial as the grain size of the material increases, which may be due to the increased interference between the flaw echo and grain noise in larger grained samples.

The unprocessed data of Figs. 6 and 7 clearly show the effects of beam spreading on the flaw echo due to the use of a nonfocused transducer. As can be seen, the processed B scans indicate that the application of the PT algorithm reduces this effect significantly.

The polarity-thresholding algorithm was also used in conjunction with LA. It was observed that PTLA provides only incremental improvement over PT and, therefore, the images are not repeated here.

V. CONCLUSIONS

A nonlinear algorithm that can be used with spatially decorrelated data to reduce the grain clutter in two-dimensional imaging has been presented. The theoretical derivations show that it is possible to achieve a significant improvement in SNR by nonlinearly processing a large number of independent spatial signals. The experimental results indicate that there is a trade-off between the SNRE attainable and the possibility of losing the flaw echo (i.e., the probability of a miss) as the spatial window size increases. This limits the sample area from which the data can be obtained, and consequently imposes an upper limit on SNRE. However,

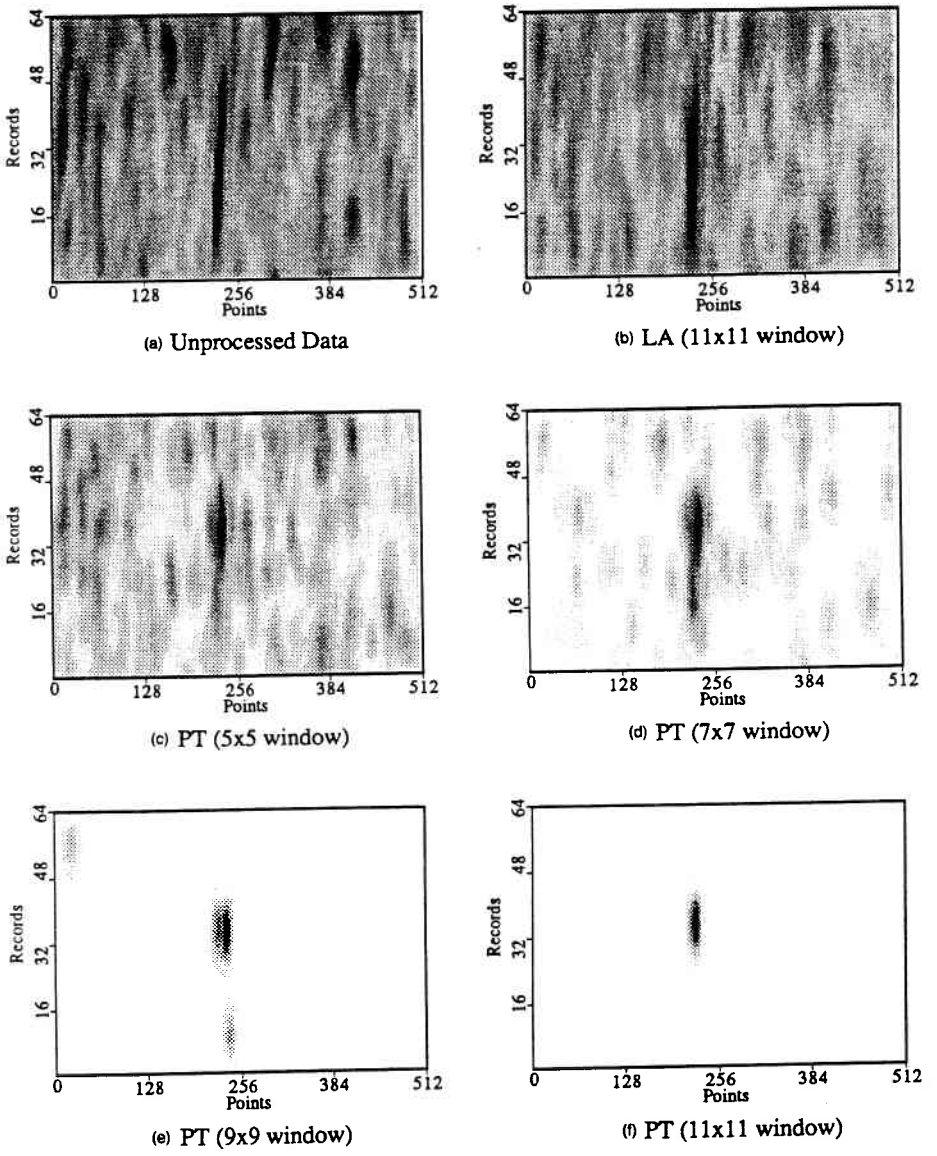

(a) Unprocessed Data (b) LA (11x11 window)

(c) PT (5x5 window) (d) PT (7x7 window)

(e) PT (9x9 window) (f) PT (11x11 window)

FIG. 7. Unprocessed and spatially processed SST75 stainless data for LA and PT.

the performance of PT was shown to be far superior to the conventional averaging technique, LA. The PT algorithm has been used successfully with samples of varying grain sizes indicating the high SNRE that can be attained experimentally.

ACKNOWLEDGMENTS

The work has been supported by NSF Grant No. ECS-8505153 and EPRI Project No. RP 2405-22.

[1]E. W. Beasley and H. R. Ward, "Quantitative Analysis of Sea Clutter Decorrelation with Frequency Agility," IEEE Trans. Aerosp. Electron. Syst. **4** (3), 468–473 (1968).

[2]P. F. Guarguaglini, "A Unified Analysis of Diversity Systems," IEEE Trans. Aerosp. Electron. Syst. **4** (2), 318–320 (1968).

[3]G. Lind, "Measurement of Sea Clutter Correlation with Frequency Agility and Fixed Frequency Radar," Philips Telecomm. Rev. **29** (1), 32–38 (1970).

[4]V. D. Koryachenko, "Statistical Processing of Flaw Detector Signals to Enhance the Signal-to-Noise Ratio Associated with Structural Reverberation Noise," Sov. J. NonDestr. Test. **11** (1), 69–75 (1975).

[5]S. Kraus and K. Goebbels, "Improvement of Signal-to-Noise Ratio for the Ultrasonic Testing of Coarse Grained Materials by Signal Averaging Techniques," National Bureau of Standard Pub. 596, 551–559 (1980).

[6]N. M. Bilgutay, J. Saniie, E. S. Furgason, and V. L. Newhouse, "Flaw-to-grain Echo Enhancement," Ultrason. Int. 152–157 (1979).

[7]N. M. Bilgutay, V. L. Newhouse, and E. S. Furgason, "Flaw Visibility Enhancement by Split-Spectrum Processing Techniques," Proc. 1981 IEEE Ultrason. Symp. 878–883 (1981).

[8]V. L. Newhouse, N. M. Bilgutay, J. Saniie, and E. S. Furgason, "Flaw-to-Grain Echo Enhancement by Split-Spectrum Processing," Ultrasonics. **20** (2), 59–68 (1982).

[9]N. M. Bilgutay and J. Saniie, "The Effect of Grain Size on Flaw Visibility Enhancement Using Split-Spectrum Processing," Mater. Eval. **42**, 808–814 (1984).

[10]I. Amir, N. M. Bilgutay, and V. L. Newhouse, "Analysis and Comparison of Some Frequency Compounding Algorithms for the Reduction of Ultrasonic Clutter," IEEE Trans. Ultrason. Ferroelectr. Freq. Control **UFFC-33** (44), 402–411 (1986).

[11]V. L. Newhouse, P. Karpur, J. L. Rose, and I. Amir, "A New Technique for Clutter Reduction in Ultrasonic Imaging," Proc. 1985 IEEE Ultrason. Symp. 998–1003 (1985).

[12]I. Amir, "Clutter Suppression and Texture Estimation in Non-Destructive Evaluation," Ph.D. thesis, Drexel University, Philadelphia, PA, (1986).

[13]U. Bencharit, J. L. Kaufman, N. M. Bilgutay, and J. Saniie, "Frequency and Spatial Compounding Techniques for Improved Ultrasonic Imaging," Proc. 1986 IEEE Ultrason. Symp. 1021–1026 (1986).

[14]N. M. Bilgutay, J. Saniie, and U. Bencharit, "Spectral and Spatial Pro-

cessing Techniques for Improved Ultrasonic Imaging of Materials" Proceedings of the NATO Advanced Research Workshop on Signal Processing and Pattern Recognition in Nondestructive Evaluation of Materials, Quebec, Canada (1987).
[15]N. M. Bilgutay, U. Bencharit, and J. Saniie, "Nonlinear Spectral Processing Techniques for Ultrasonic Imaging," Proceedings of the 1987 Progress in Quantitative NDT (1987).
[16]V. L. Newhouse, J. L. Rose, P. Karpur, and P. M. Shankar, "Split Spectrum Processing: Performance of the Polarity Thresholding Algorithm in Signal-to-Noise Ratio Enhancement In Ultrasonic Applications," Proceedings of the 1987 Progress in Quantitative NDT (1987).
[17]A. Papoulis, *Probability, Random Variables, and Stochastic Processes* (McGraw-Hill, New York, 1984).
[18]J. G. Abbott and F. L. Thurstone, "Acoustic Speckle: Theory and Experimental Analysis," Ultrason. Imag. **1**, 303–374 (1979).
[19]C. B. Burckhardt, "Speckle in Ultrasound B-Mode Scans," IEEE Trans. Sonics Ultrason. **SU-25** (1), 1–6 (1978).
[20]S. M. Gehlbach, "Quantitative Analysis of Acoustical Speckle," Ultrason. Imag. **5** (2), 190–194 (1983).
[21]G. E. Trahey, S. W. Smith, and O. T. Von Ramm, "Speckle Pattern Correlation with Lateral Aperture Translation: Experimental Results and Implications for Spatial Compounding," IEEE Trans. Ultrason. Ferroelectr. Freq. Control **UFFC-33** (3), 257–264 (1986).